Observations of Satellites Using Near-Simultaneous Polarization Measurements

Audra M. Jensen, Michael K. Plummer, Daniel S. O'Keefe, Francis K. Chun
Department of Physics, US Air Force Academy, USAF Academy, CO
David M. Strong
Strong EO Imaging, Inc., Colorado Springs, CO 80908

ABSTRACT

The United States Air Force Academy operates an f/8.2 16-inch telescope fitted with an Andor Alta U47 1024×1024 pixel CCD camera and a nine-position filter wheel. In 2019, 2020, and 2021, we used this telescope to observe geosynchronous communication satellites during the glint season, which occurs around the fall and spring equinoxes. We captured near-simultaneous polarization images of several clusters of operational geosynchronous communication satellites using linear polarization filters with specific orientations (0°, 45°, 90°, 135°) relative to the CCD camera's vertical axis. We converted the measured intensities through these filters to determine the first three Stokes parameters (S_0, S_1, S_2) of the light reflecting off the satellites and incident to the telescope. A first-order time-series analysis of the Stokes parameters indicated that some of the collected data was corrupted, presumably by clouds. To determine if this was true, we developed a technique that quantifies the correlation between pairs of satellites appearing in the same raw image, allowing us to unambiguously confirm when the collected data was corrupted. We processed the remaining data and found a distinct difference between a satellite's polarization signature during a glint versus its signature outside of the glint period.

1. INTRODUCTION

Space has become a vital area of operations in the United States for military, civil, and commercial reasons. Our space enterprises give us an asymmetric advantage in the international community, and our competitors are seeking to close the gap. Consequently, on 20 December 2019, the United States Space Force (USSF) was established as a separate military branch under the Department of the Air Force. Almost weekly, events occur that support Space Force operations, such as delta formation (which are the Space Force equivalent of an Air Force group or wing), doctrine release, and members of the Space Force deploying for the first time. In April of 2020, the first class of officers from the United States Air Force Academy commissioned directly into the United States Space Force. These became the third through eighty-eighth Space Force members, after the Chief of Space Operations and the Chief Master Sergeant of the Space Force who were the first two. Since then, more than 2,400 active duty airmen transferred into the Space Force starting on 1 September 2020 [1].

Now more than ever, space situational awareness (SSA) and space domain awareness (SDA) are higher priorities to the United States' national security. SSA is "the requisite foundational, current, and predictive knowledge and characterization of space objects" [2]. It depends on "integrating space surveillance, collection, and processing; status of US and cooperative satellite systems; understanding of US and multinational space readiness; and analysis of the space domain" [2]. SSA was the term that the United States Space Command used until 4 October 2019, when they switched to using SDA to emphasize space as a warfighting domain. The definition of SDA is more active than passive and addresses the security of the United States. In the publication *Spacepower*, SDA is defined as "the effective identification, characterization, and understanding of any factor associated with the space domain that could affect space operations and thereby impacting the security, safety, economy, or environment of our Nation" [3]. SDA is a core competency of the Space Force and it supports the cornerstone responsibilities of preserving freedom of action, enabling joint lethality and effectiveness, and providing independent options [3]. The Space Force realizes that the space domain is imperative to the success of missions in other domains and that space supremacy ensures our nation's security.

A monumental improvement in SDA, going beyond orbit determination, would be the ability to more fully characterize a satellite from the surface of the earth based solely on optical data from a telescope. A resolved image can provide information about a satellite and its characteristics (e.g. size, shape, orientation materials), but to obtain resolved images at orbital distances requires either a very large aperture telescope or a very large satellite.

PA#: USAFA-DF-2021-254

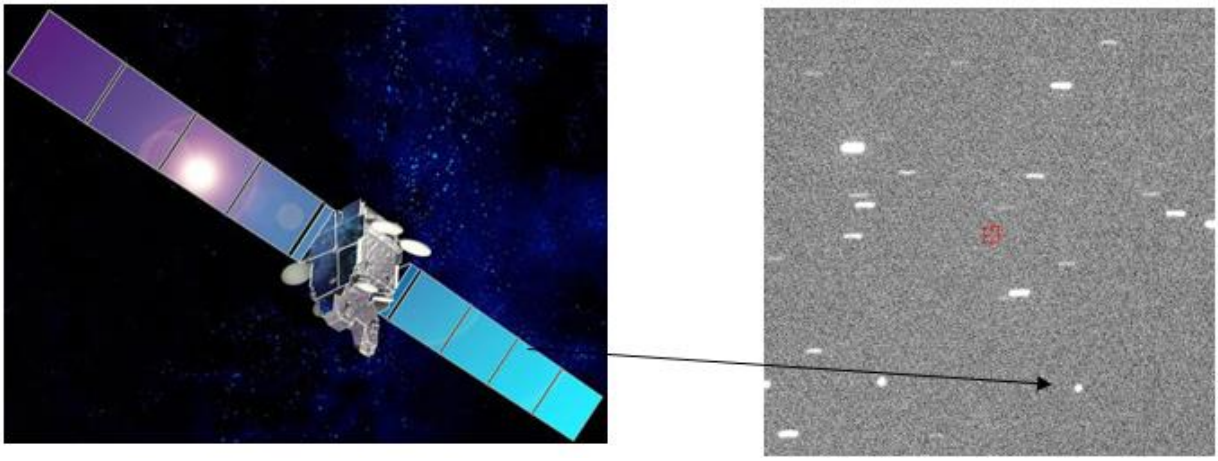

Fig. 1: Artist rendition of WildBlue-1 (left) and WildBlue-1 (right) as an unresolved point source [4].

Since telescope apertures of this size are expensive to build and operate, the satellites we observe must be treated as unresolved point sources. However, using standard astronomical techniques, there are methods to characterize satellites from their point source image. Many of these techniques focused primarily on a satellite's photometric and spectral signatures. In the early years of the space age, researchers measured satellite optical properties to determine orbits and temperature [5-6] and visible reflectance spectra [7]. Specific to geosynchronous (GEO) satellites, broadband photometry was used to classify geosynchronous satellites [8], determine their solar panel offsets [9], and survey features of solar panel glints [10]. Spectral measurements of space debris in GEO orbits showed that despite exhibiting a night-to-night variation, their overall spectral shape was maintained [11]. Spectra of GEO satellite glints also confirmed the satellite solar panels as the source of the glint [12]. However, it was also found to be the case, that caution must be taken when combining spectral measurements obtained over different nights because solar phase angle can significantly impact the observed spectrum [13].

Polarization measurements of satellites, however, have not been exploited to the same degree as photometry and spectroscopy. An early study looked at the polarization signature of one satellite (Space Object #893) which showed a maximum of 39% polarization noting that the plane of polarization was perpendicular to the plane of incidence as expected by Brewster's Angle [14]. More recently, polarimetry analysis conducted on satellites demonstrated that polarization signatures can characterize and distinguish different types of operational communication satellites in GEO [15]. The goal of this project is to explore the efficacy of polarization measurements to more fully characterize geosynchronous satellites. Measurements of near-simultaneous polarization can potentially provide information about the surface material composition of a satellite and help us distinguish one satellite from another. Also, by comparing features in a satellite's polarization signature to corresponding spectral and/or photometric signatures, we may be able to gain further physical insight of a satellite.

2. INSTRUMENTATION AND PROCESSING

The linear polarization of light can be fully characterized by the first three Stokes Parameters, where S_0 is the total intensity of the light, S_1 is the preference towards a vertical or horizontal polarization, and S_2 is the preference towards a diagonal polarization. The parameters allow us to quantify the degree and angle of linear polarization, and compare them between different satellites, different days of observation, and different satellite properties. The equations for these parameters are given by

$$S_0 = \frac{I_0+I_{45}+I_{90}+I_{135}}{2} \quad (1)$$

$$S_1 = I_0 - I_{90} \quad (2)$$

$$S_2 = I_{45} - I_{135} \quad (3)$$

In 2019, we installed and calibrated a new linear polarimeter on the 16-inch telescope at the USAFA observatory [18]. The polarimeter consists of four linear polarization filters from American Polarizers Inc., model number AP42-

100G-AR2, which provide a 44% single-pass transmission between 400-700 nanometers. The filters or polarization analyzers were placed into four empty slots in an existing nine-position filter, oriented at angles of 0°, 45°, 90°, and 135° relative to the vertical axis of the camera's focal plane. The calibration source consisted of a uniform, unpolarized light source (e.g. Alnitak Flatman light panel) and a polarized film acting as a generator. The calibration flat images followed Malus' Law well, allowing the determination of the polarization calibration matrix which accounts for the polarization effects within the telescope optical train. This calibration matrix now allows us to convert measured camera intensities through the four filters to three satellite Stokes parameters, S_0, S_1, and S_2.

Previous cadets used this telescope during several equinoctial periods to observe communication satellites in geosynchronous orbit. The experimental setup is illustrated in the Fig. 2 below. Unpolarized light from the sun reflecting off the surface of a satellite can become partially polarized. In effect, the satellite acts as a generator of polarized light. As this light enters the telescope, it reflects off the primary and secondary mirrors of the telescope, passes through the polarization filter or analyzer, and its intensity is measured by the CCD camera which is assumed to be polarization agnostic.

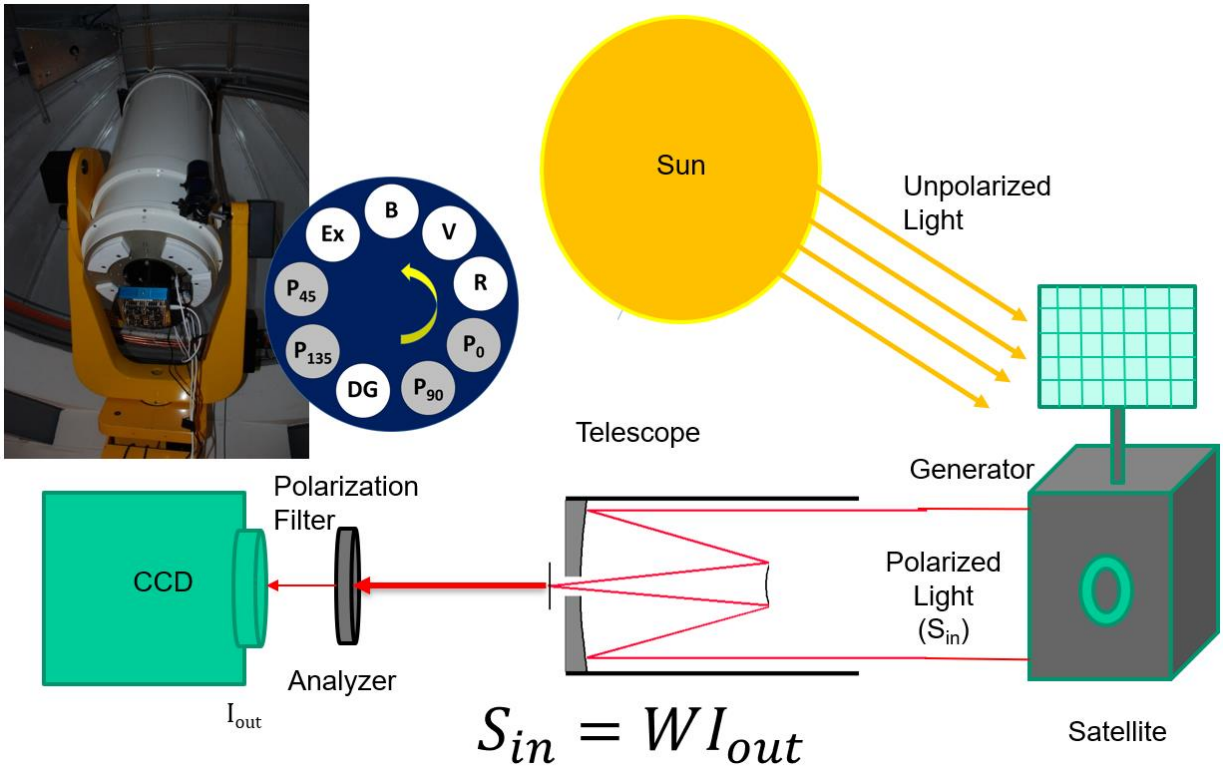

Fig. 2: Experimental setup of observations [19]

After observations were made, the data measurements for each satellite were processed according to the flow chart shown in Fig. 3.

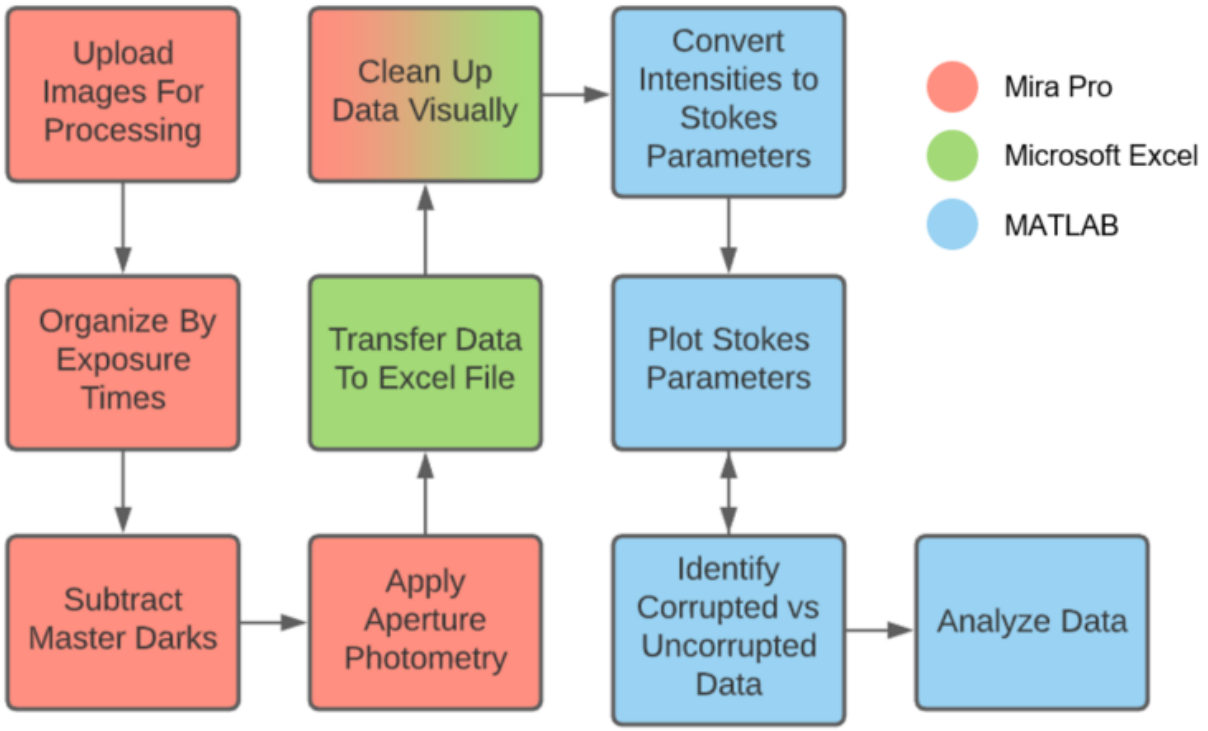

Fig. 3: Data processing flow chart

First, we uploaded the satellite images into an astronomical commercial program called Mira® Pro™, allowing us to organize them by exposure times. Next, we subtracted the corresponding master dark from the satellite images to eliminate the thermal electron noise (or dark current) from the science images. These master darks were taken during that particular glint season and separate darks were taken for each exposure time used. After the master darks were subtracted, we used Mira Pro's aperture photometry tool to measure the signal counts of the satellite, taking into account the background noise, and exported the data to a Microsoft Excel file for ease of transfer to MATLAB®. Some of the information in this Excel file was the magnitude of the satellite, location in the image, net counts, background counts, exposure time, date and time, and filter. Before we imported the Excel file into MATLAB, we cleaned up the data visually, which consisted of inspecting each image in Mira Pro one by one and deleting corrupted data points. These corrupted images could be due to poor tracking of the telescope, a star that crossed behind the satellite and changed the counts, or incorrect processing of the satellite through Mira Pro. After these corrupted images were identified, we deleted these data points from the Excel file.

Next, we converted the intensities into the correct Stokes Parameters using a polarization calibration matrix (referred to as the *W* matrix), which accounts for the effect of the telescope's optical elements on the polarization of incident light. Plotting the Stokes Parameters as a function of time, we again inspected the data and deleted any corrupted images. For example, if we saw an unexpected spike in S_0, we went back through the data and discovered that the satellite was either tracked improperly for that image or there was a star trail passing close to the satellite.

3. IMPACT OF CLOUDS

When we analyzed and compared glinting satellite data taken during the 2020 vernal equinox, we observed that Spaceway-3 (SW3) data taken on 12 March 2020 exhibited much larger variation in S_1 and S_2 than other satellite polarization data taken on different days. The observation log indicated that clouds were present on 12 March 2020, which would potentially corrupt the data. To investigate, we exploited the fact that there were other satellites captured in the image with SW3: IntelSat-30 (IS30), IntelSat-31 (IS31), and Galaxy3C (G3C), as seen in Fig. 4.

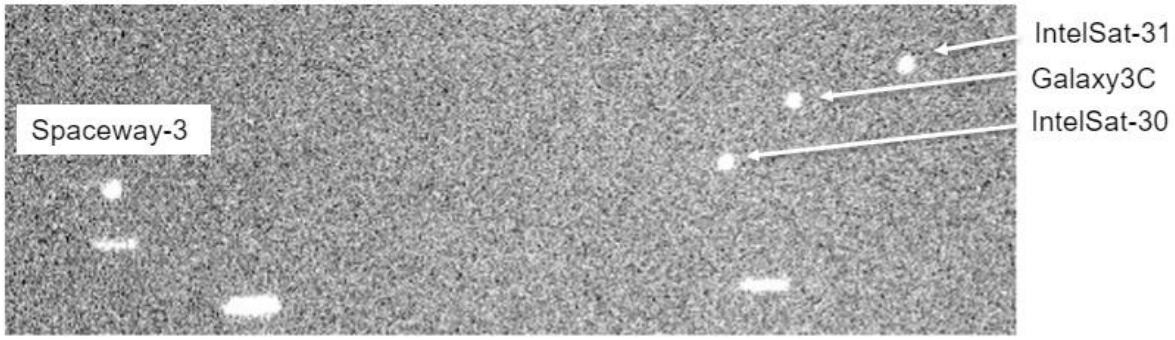

Fig. 4: Raw subframe image of data collected on 12 March 2020

By comparing the time series plots of the four satellites in the 12 March 2020 cluster, shown in Fig. 5, we observe that the S_0 signals (black trace) of the three non-glinting satellites (i.e. all except Spaceway-3) appear to show the same pattern. If the glinting satellite (Spaceway-3) were on the same scale for its y-axis as the others, we suspect that a similar pattern would be visible.

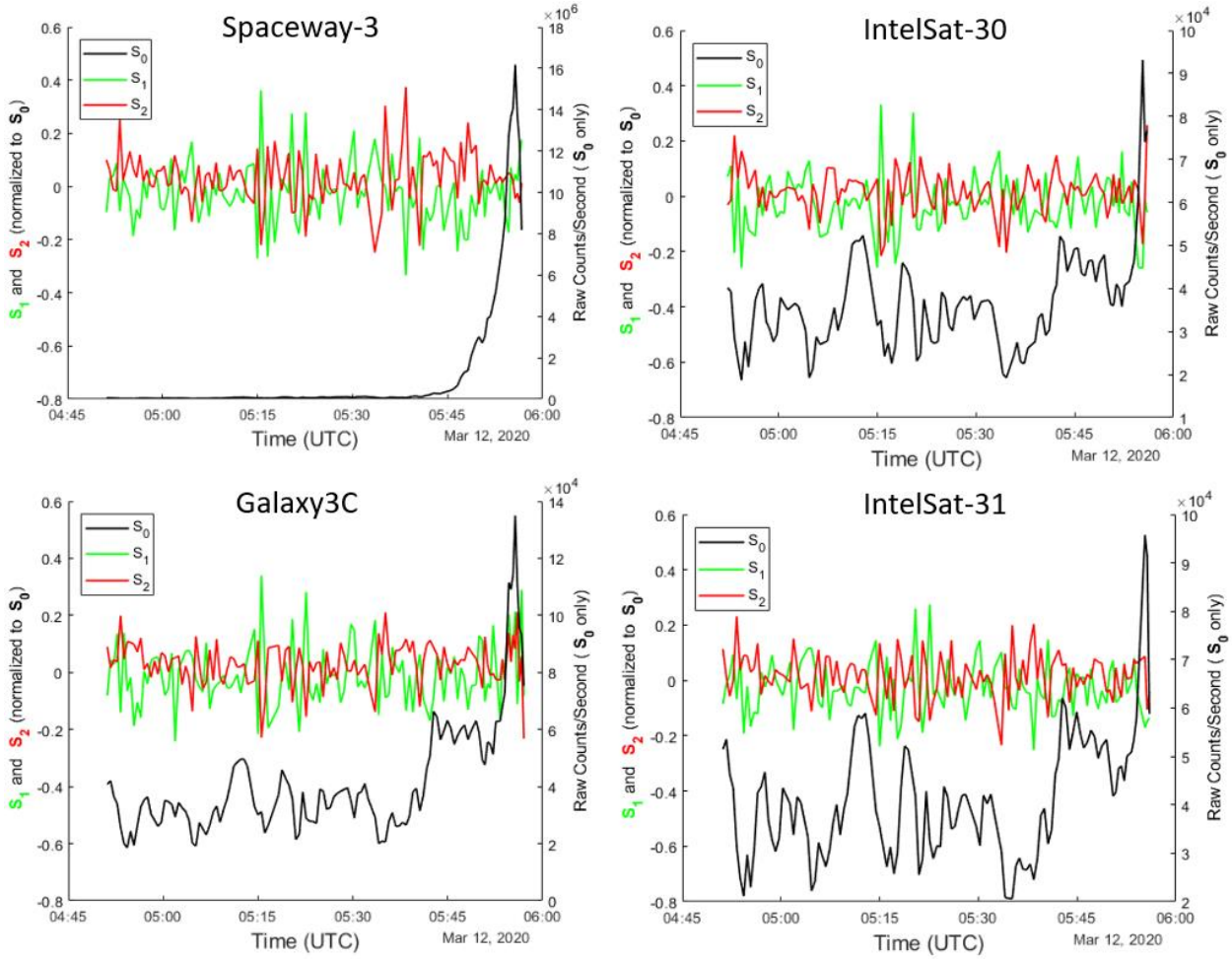

Fig. 5: The time series of each of the satellites from the 12 March 2020 cluster: Spaceway-3 (upper left), IntelSat-30 (upper right), Galaxy3C (lower left) and IntelSat-31 (lower right). In all four time series plots, S_0 is the black trace and follows the right vertical axis, and S_1 and S_2 are the green and red traces, respectively, and follow the left vertical axis.

To further investigate, we plot the S_1 and S_2 as a function of time separately for this cluster to determine if there is any similarity in their data variability. Because all the satellites in this cluster appear to exhibit similar profiles, Fig. 6 shows that the variability in the polarization data is not a function of the satellites, but of the image itself. This could be from clouds or another atmospheric condition affecting the polarization signatures from all the satellites in the image. Either way, this data appears corrupted because we can reasonably expect individual satellites in a cluster to have different polarization signature profiles.

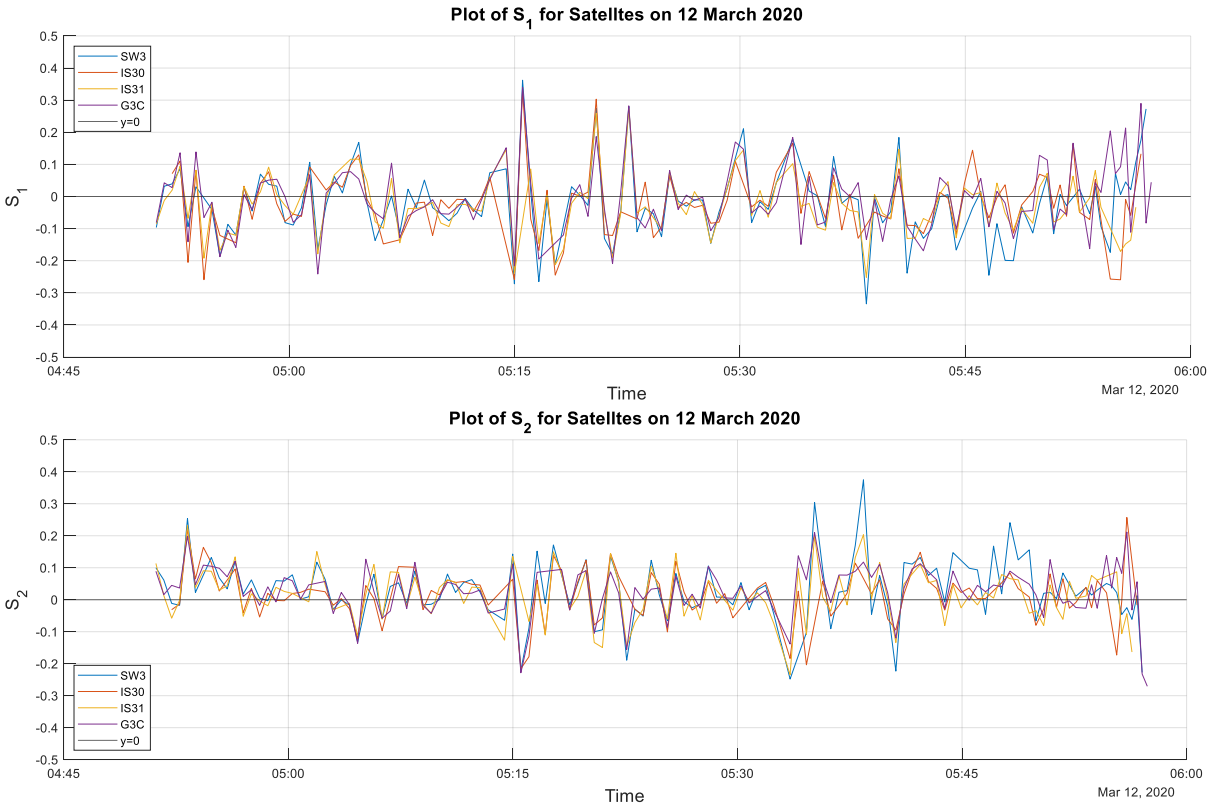

Fig. 6: Time series plot of S_1 (upper plot) and S_2 (lower plot) for the 12 March 2020 cluster.

Furthermore, when we analyzed a scatterplot of the S_1 (or S_2) of one satellite versus the S_1 (or S_2) of another satellite in that same cluster, we observed a strong correlation. Of the twelve possible unique pairings of the four satellites per the S_1 and S_2 parameters, Fig. 7 shows four examples: IntelSat-30 vs. IntelSat-31 (S_1 and S_2 separately) and Galaxy3C vs. Spaceway-3 (S_1 and S_2 separately).

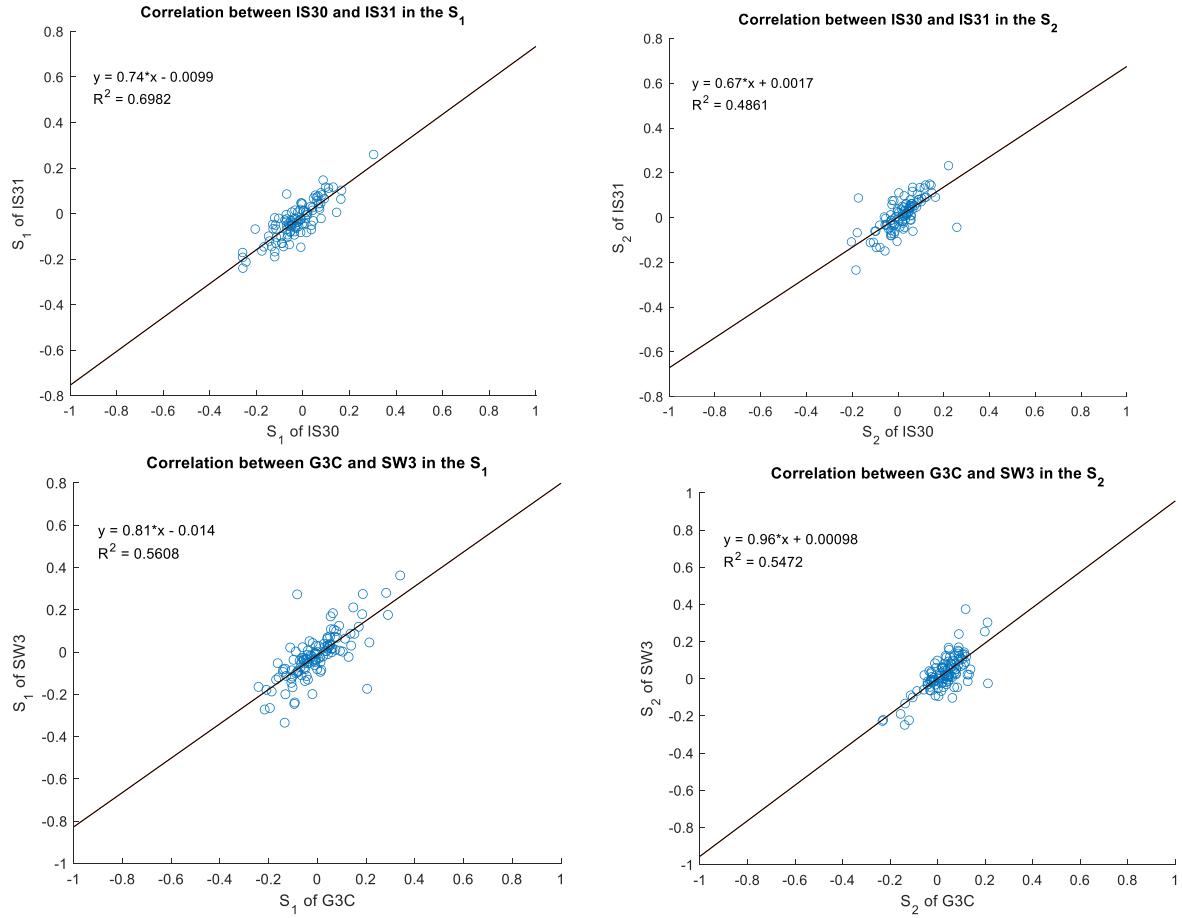

Fig. 7: Plots of the correlation between S_1 and S_2 of IS30 and IS31 (upper plots) and of G3C and SW3 (lower plots). Data from these satellites were all taken on 12 March 2020.

From the results of the linear regressions in Fig. 8, we observe that all of the plots have an R^2 ranging from 0.4861 to 0.6982. Since an R^2 value of 1 indicates that two datasets are perfectly correlated and a value of 0 indicates that the data is uncorrelated, we conclude that these polarization signatures of the 12 March 2020 cluster are more correlated and thus corrupted. This step to determine the correlation and possible corruption of satellite data was included as the second to last step in the data processing flow shown earlier in Fig. 3.

As a final check of our approach to determine whether any satellite results were corrupted, Fig. 8 shows an example of data deemed uncorrupted and thus useable for the DirecTV (DTV) cluster observed on 22 October 2019. A low correlation between DTV10 and DTV15 was determined, as the R^2 values were 3.56×10^{-6} and 0.025 respectively. For perfectly uncorrelated data, we would expect an R^2 of zero and a slope of either zero or infinity which is the case for DTV10 and DTV15.

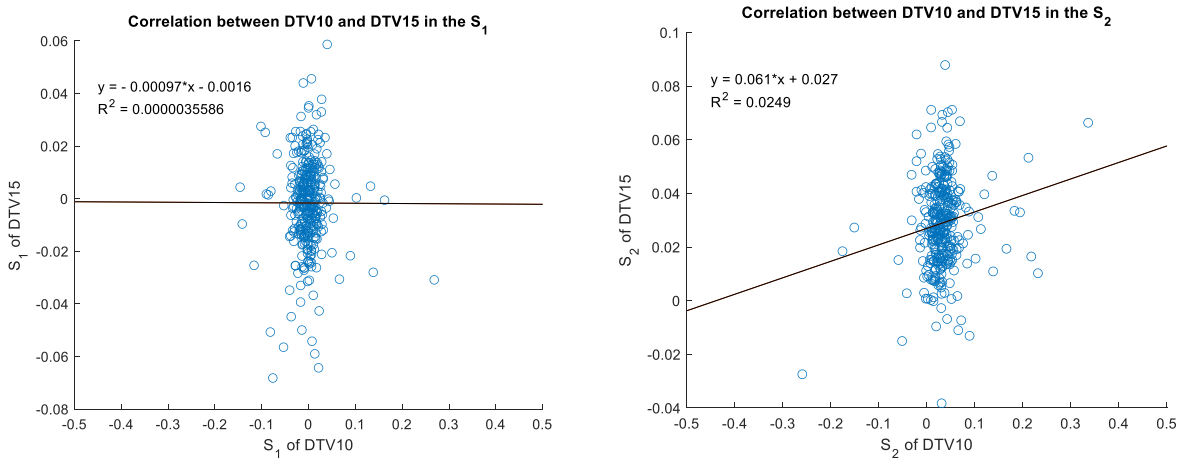

Fig. 8: Plots of the correlation between S_1 (left) and S_2 (right) for DTV10 and DTV15 observed on 22 October 2019.

4. RESULTS

During the glint seasons of October 2019, March 2020, February-March 2021, cadets took polarization data of several satellites across multiple nights [19-20]. Those observations where satellite data was uncorrupted and when the satellites exhibited a strong glint are shown in Table 1 below, along with corresponding satellite attributes. We defined a strong glint as an intensity of 10^6 or greater counts per second, a weak glint as an intensity of about 10^5 counts per second, and a no glint as an intensity of 10^4 counts per second. Based on average distances between the Sun, the satellite, and the Earth, the strongest intensity in the glint is approximately 334 km by 16.7 km on the ground, consistent with other estimates [10]. This is calculated with the Sun being an extended light source and the assumption that the satellite is a 40-m by 2-m plane mirror. Different solar panel arrangements will create a different shape of the reflection on the ground. Outside of this peak area, the intensity falls off because less of the Sun is reflected at distances further from the peak spot. This has been seen in weaker glints when the alignment is not sufficient to place the ground observation location within the peak area. Since stronger-glinting satellites had larger intensity signals, the polarization signatures tended to be stronger and more easily studied.

Table 1: List of uncorrupted polarization data collections for stronger glinting satellites observed during 2019-2021 equinoxes and corresponding satellite attributes.

Satellite	Date of Glints	S/C Vendor	S/C Bus	Launch Date	Estimated Size	Mass
DTV-10	22-Oct-2019	Boeing	BSS-702	6-Jul-2007	140 m^2	5893 kg
	23-Feb-2021					
DTV-15	22-Oct-2019	Airbus	Eurostar-3000	27-May-2015	140 m^2	6205 kg
	3-Mar-2020					
DTV-14	11-Mar-2020	SS/L	SSL-1300	6-Dec-2014	140 m^2	6300 kg
	3-Mar-2021					
	4-Mar-2021					
SES-3	11-Oct-2020	Orbital Sciences Corporation	Star-2.4	15-Jul-2011	120 m^2	3170 kg
	13-Oct-2020					
AMC-15	4-Oct-2019	Lockheed	A2100A	14-Oct-2004	80 m^2	4021 kg
WB-1	4-Mar-2020	SS/L	SSL-1300	8-Dec-2006	80 m^2	4735 kg

The time series plots of DTV-10 for 22 October 2019 (left plots) and 23 February 2021 (right plots) are shown in Fig. 9, with the overall intensity, S_0 (blue trace), and degree of linear polarization (DOLP, red trace) shown in the upper plots, where

$$\mathrm{DOLP} = \sqrt{\frac{S_1^2 + S_2^2}{S_0^2}}. \tag{4}$$

The bottom plots in Fig. 9 also show the DOLP (red trace), but they also show the angle of linear polarization (AOLP, blue trace) of the satellite's polarization signature, where

$$\mathrm{AOLP} = \frac{1}{2}\tan^{-1}\left(\frac{S_2}{S_1}\right). \tag{5}$$

The uncertainties were derived from propagating the uncertainty error in the intensity measurements, which follow Poisson statistics. Comparing the overall intensities (blue traces in upper plots) for the two different observation nights, we see that the glint on 22 October 2019 occurs at approximately 06:30-06:40 UTC and peaks to 3.7×10^7 counts per second while the glint on 23 February 2021 occurs at approximately 06:50-07:15 UTC and peaks to 6.5×10^7 counts per second. During both glints, we see that the strength of the polarization signature (red trace) increases from less than 0.05 to 0.34 on 22 October 2019 and to 0.24 on 23 February 2021. Thus, during the glint, the strength of the light reflected off the satellite not only increases by a factor of a hundred, but so does the proportion of that signal that is linearly polarized. By combining these two effects, we observe that the linear polarization signal from the DTV-10 satellite is nearly one thousand times stronger during a glint. Besides the strength of the polarization during a glint, we can also take note of the direction of the polarization signal (blue trace in lower plots). We see that for the 22 October 2019 collection, the AOLP for DTV-10 tended to be centered around 45° before and after the glint and oscillate rapidly throughout most of the angle range during the glint. On 23 February 2021, the AOLP also oscillates rapidly during the glint, but outside of the glint it tended to be centered around -75° before the glint and 60° after the glint. Since the observation on 22 October 2019 utilized only the four polarization filters, it has twice the temporal resolution of the observation on 23 February 2021, which also included a diffraction grating, B, V, and R filters.

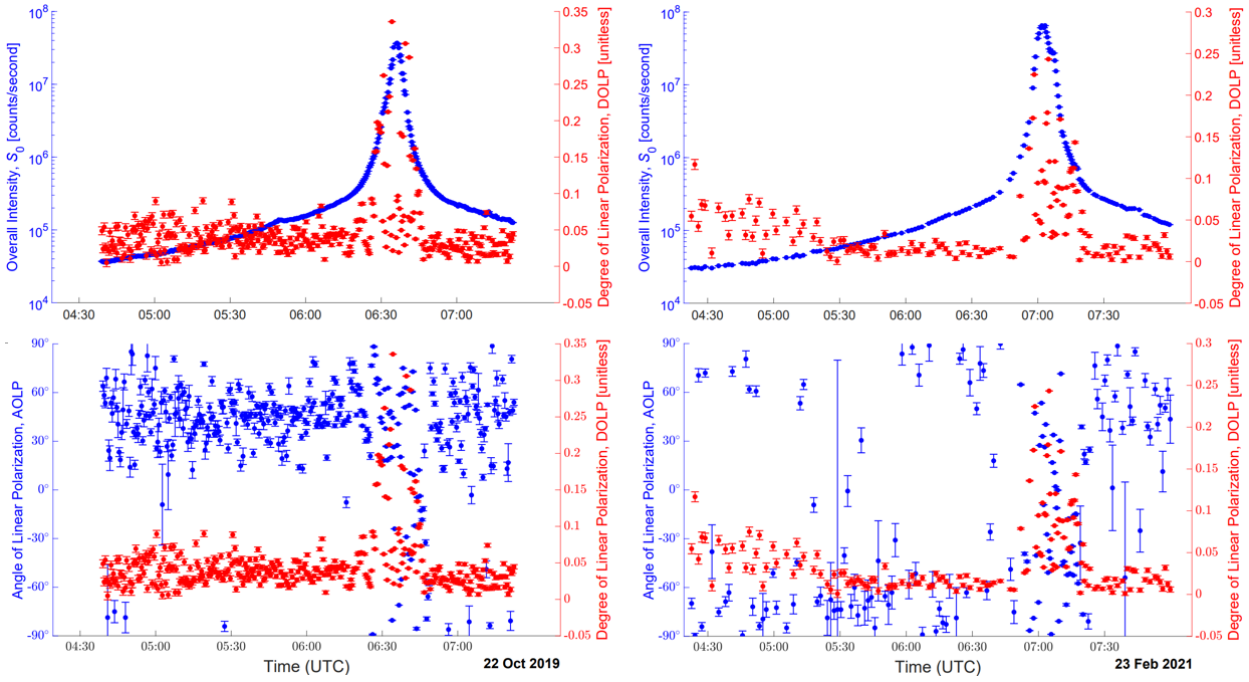

Fig. 9: Polarization results of DTV-10 observed between 04:30-07:30 UTC on 22 October 2019 (left) and between 04:30-08:00 UTC on 23 February 2021 (right). Top: Plots of the overall intensity S_0 (blue trace) in raw counts per second along with DOLP (red trace). The satellite glints from approximately 06:30-06:40 UTC on 22 October 2019 and from approximately 06:50-07:15 UTC on 23 February 2021. Bottom: Plots of the AOLP (blue trace) and DOLP (red trace) for the same timeframes.

The time series plots of DTV-15 for 22 October 2019 (left plots) and 3 March 2020 (right plots) are shown in Fig. 10. The overall intensity (blue trace) for the 22 October 2019 observation shows a double glint (i.e. two periods where there was a significantly stronger S_0 signal). For the 3 March 2020 time series plot, the later half of the glint was not recorded, and only the period leading up the glint is shown. While both of these observations could be categorized as strong glints (i.e. they had peaks of 1.2×10^6 counts per second and 8.3×10^6 counts per second), the peaks were an order of magnitude weaker than for DTV-10. Furthermore, while a stronger DOLP signal was generally observed during the glint for each case (peaking to 0.10 and 0.09), DOLP was similarly not near as strong as it had been for DTV-10 (which had a DOLP from 0.24-0.34). This relationship is the first example suggesting that the fraction of light that is polarized during a glint seems to be correlated with the overall signal intensity; a feature that we will explore in-depth after presenting the rest of the satellite polarization data. As was for DTV-10 on 23 February 2021, the AOLP had a cluster of points around -75° before the glint and had significant variation during the glint period. On 22 October 2019 we also observed a positive AOLP after the glint, but this time around 30°.

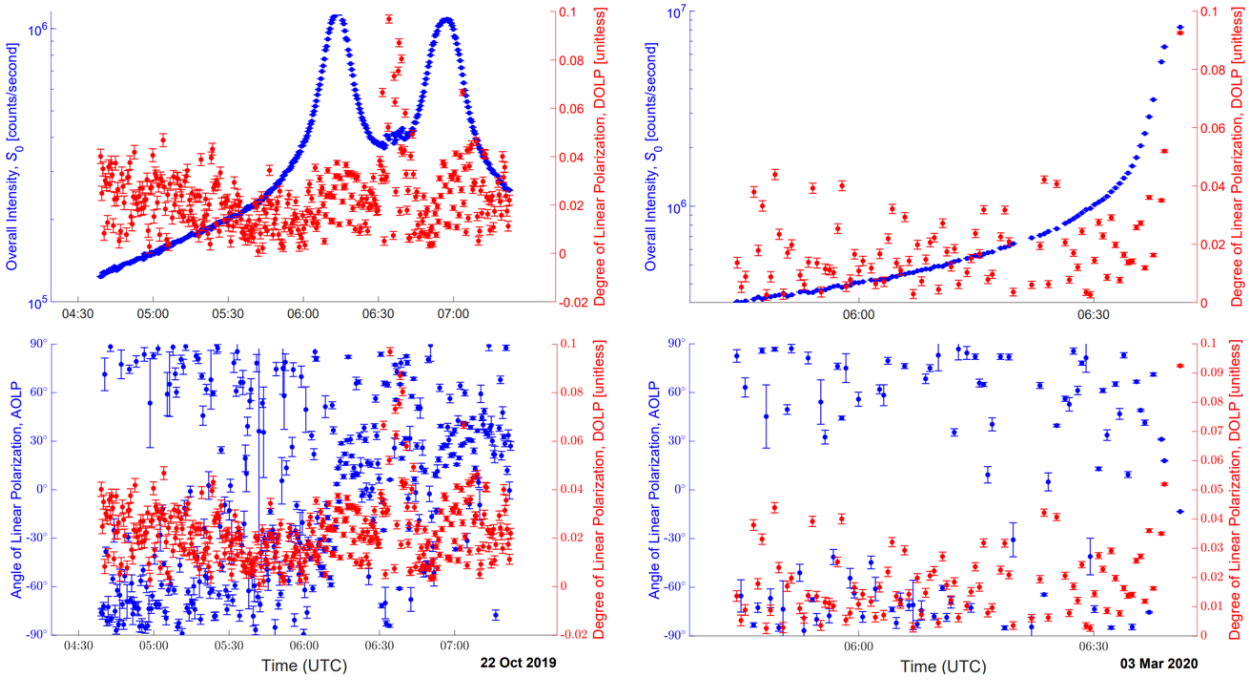

Fig. 10: Polarization results of DTV-15 observed between 04:30-07:30 UTC on 22 October 2019 (left) and between 05:45-06:40 UTC on 3 March 2020 (right). Top: Plots of the overall intensity S_0 (blue trace) in raw counts per second along with DOLP (red trace). The satellite glints twice from approximately 06:00-06:20 UTC and 06:45-07:10 UTC on 22 October 2019 and once beginning from approximately 06:35 UTC on 3 March 2020. Bottom: Plots of the AOLP (blue trace) and DOLP (red trace) for the same timeframes.

The time series plots of DTV-14 for 11 March 2020 (left plots), 3 March 2021 (center plots), and 4 March 2021 (right plots) are shown in Fig. 11. The peak intensity of this satellite ranges from 5.2×10^6 counts per second taken on 11 March 2020 to 1.3×10^8 counts per second taken on 4 March 2021, which was one of the strongest glints we have observed to date. The 3 and 4 March 2021 observations were of a double glint, while the 11 March 2020 observation was only of a single glint; we are currently exploring whether the smaller precursor to the main glint for these two nights is present in photometric and spectral data taken on the same night. As might be expected from a possible correlation between peak overall signal and peak polarization signal, the DOLP for 11 March 2020 has a maximum of only 0.09, while the DOLP on 3 and 4 March 2021 reaches 0.26 and 0.42 respectively. It is worth noting there is a gap in data from about 06:25-07:15 UTC on 3 March 2021; this occurred because of the satellite going into the Earth's shadow. Finally, the pre-glint AOLP for all three observations showed similar results as previously discussed satellites: a negative AOLP before the glint, significant variability in AOLP during the glint when the linear polarization signal is strongest, and a positive AOLP following the glint.

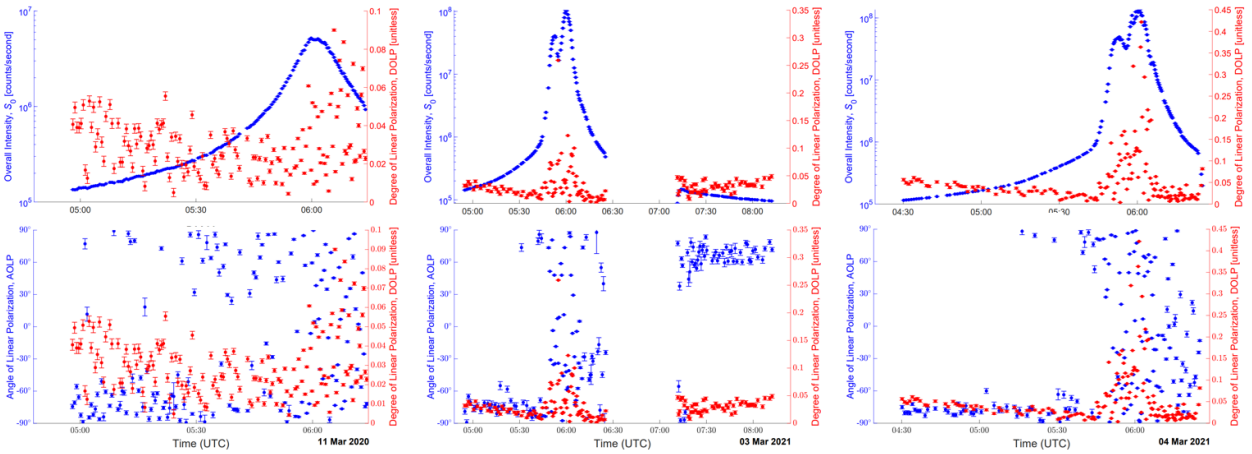

Fig. 11: Polarization results of DTV-14 observed between 05:00-06:15 UTC on 11 March 2020 (left), between 05:00-08:00 UTC on 3 March 2021 (center), and between 04:30-06:15 on 4 March 2021 (right). Top: Plots of the overall intensity S_0 (blue trace) in raw counts per second along with DOLP (red trace). The satellite glints from approximately 05:50-06:10 UTC on all three dates. Bottom: Plots of the AOLP for the same timeframes.

The time series plots of SES-3 for 11 October 2020 (left plots) and 13 October 2020 (right plots) are shown in Fig. 12. The peak intensity of this satellite ranges from 9.5×10^6 counts per second taken on 13 October 2020 to 1.8×10^7 counts per second taken on 11 October 2020. The 13 October 2020 observation includes a double glint, while 11 October 2020 only had a single glint, which seems to have been captured between a double glint. The gaps in data from 06:25-07:00 UTC on 11 October 2020 and from 06:25-06:50 UTC on 13 October 2020 were due to the satellite going into the Earth's shadow. Both collections demonstrated unusual behavior in overall intensity approximately an hour after the final peak, where it briefly rises, suggesting a unique geometric figure on the SES-3 satellite compared to the other satellites observed. Since these two observations captured a large span of the post-glint period, it was helpful to compare the post-glint AOLP with the previous figures. As before we observe that the AOLP tends to take on more positive values after the glint.

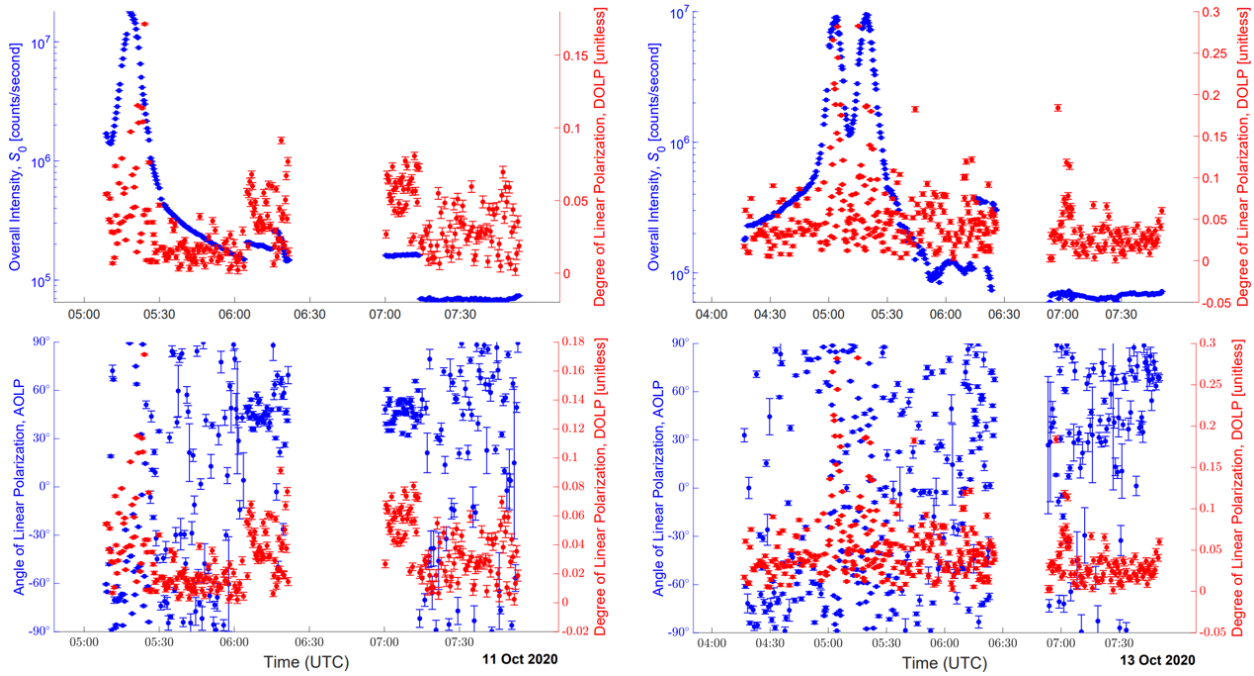

Fig. 12: Polarization results of SES-3 observed between 05:00-08:00 UTC on 11 October 2020 (left) and between 04:30-07:45 on 13 October 2021 (right). Top: Plots of the overall intensity S_0 (blue trace) in raw counts per second

along with DOLP (red trace). The satellite glints from approximately 05:00-05:30 UTC on both dates. Bottom: Plots of the AOLP (blue trace) and DOLP (red trace) for the same timeframes.

The time series plots of AMC-15 on 8 October 2019 (left plots) and of WB-1 on 4 March 2020 (right plots) are shown in Fig. 13. The peak intensity of both satellites was around 3.3×10^6 counts per second, with peak DOLPs of 0.11 for AMC-15 and 0.08 for WB-1. The DOLP was unusual for WB-1, as it seemed to decrease leading up to the glint. Both satellites captured AOLP trends observed previously, where the pre-glint AOLP is centered around -75° and AOLP exhibits increased variability during the glint.

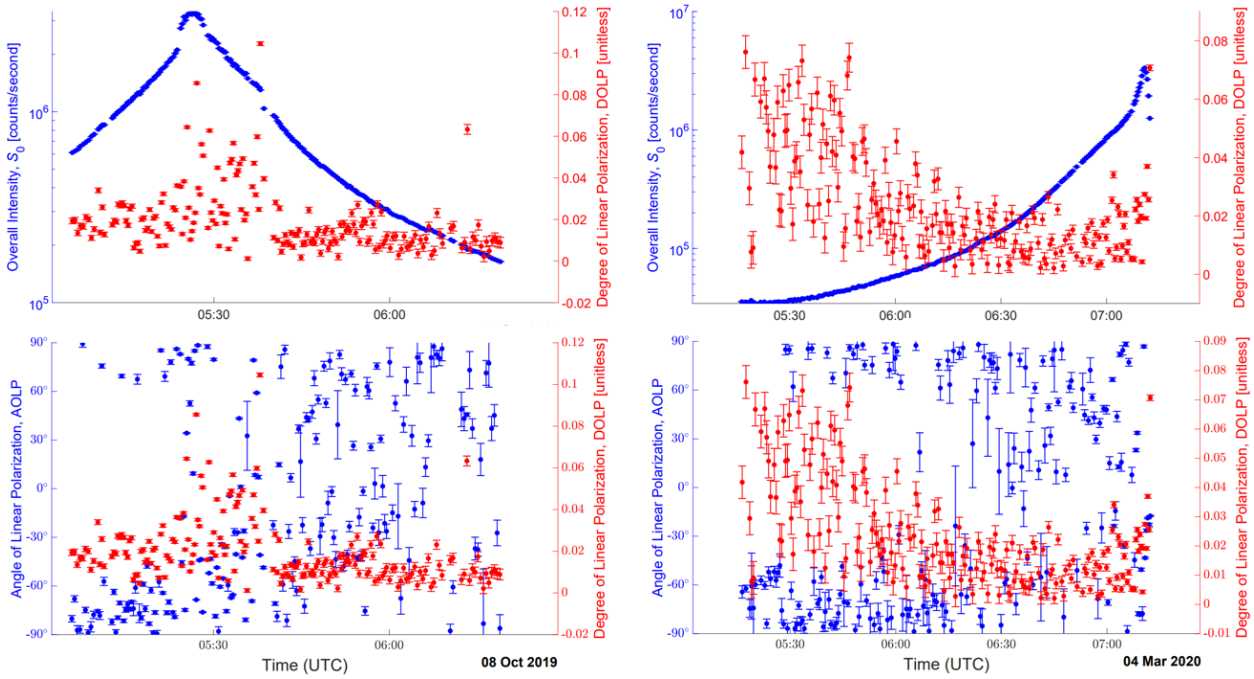

Fig. 13: Polarization results of AMC-15 observed between 05:00-08:15 UTC on 8 October 2019 (left) and of WB-1 between 05:15-07:15 on 4 March 2020 (right). Top: Plots of the overall intensity S_0 (blue trace) in raw counts per second along with DOLP (red trace). AMC-15 glints from approximately 05:20-05:40 UTC, while WB-1 glints from approximately 07:00-07:15 UTC. Bottom: Plots of the AOLP (blue trace) and DOLP (red trace) for the same timeframes.

From each of the time series plots (Fig. 9-13), the peak S_0 and peak DOLP are plotted in Fig. 14. A linear trendline corresponding to all (Peak S_0, Peak DOLP) data points is plotted in blue, while a linear trendline corresponding to only the DTV satellite data (i.e. DTV-10, DTV-14, and DTV-15) is plotted in orange. When incorporating all satellite data, the R^2 value is 0.61, however with only using the DTV satellite data, the R^2 value is 0.71. These results suggest a correlation between the peak signal strength during a glint and the fraction of light that is linearly polarized and that this correlation depends on the type of satellite. If the relation between peak S_0 versus the peak DOLP indeed depends on underlying physical features of a satellite (e.g. the sizes of the satellite bus and solar panels), then it may be possible to estimate satellite physical characteristics by looking at the trendline of unresolved satellite data on multiple nights.

Satellite	Date	Peak S_0	Peak DOLP	Size (m^2)
DTV-10	22-Oct-19	3.7E+07	0.34	140
DTV-10	23-Feb-21	6.5E+07	0.24	140
DTV-15	22-Oct-19	1.2E+06	0.10	140
DTV-15	3-Mar-20	8.3E+06	0.09	140
DTV-14	11-Mar-20	5.2E+06	0.09	140
DTV-14	3-Mar-21	1.0E+08	0.26	140
DTV-14	4-Mar-21	1.3E+08	0.42	140
SES-3	11-Oct-20	1.8E+07	0.17	120
SES-3	13-Oct-20	9.5E+06	0.28	120
AMC-15	8-Oct-19	3.3E+06	0.11	80
WB-1	4-Mar-20	3.3E+06	0.08	80

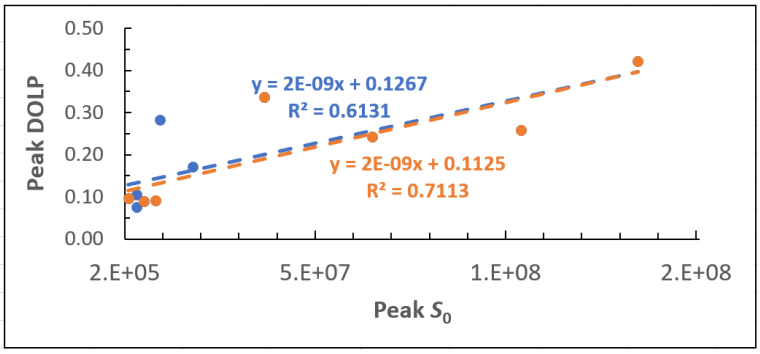

Fig. 14: Plot of the peak S_0 versus the peak DOLP from all satellite time series data. The orange data points and trendline correspond to only the DTV satellite data (i.e. DTV-10, DTV-14, and DTV-15), while the blue points include SES-3, AMC-15, and WB-1.

The difference in the polarization signal's DOLP and AOLP between glint and non-glint phases also hints at underlying phenomenological differences. This signal difference is often manifested as an increase in the DOLP and a more rapid AOLP variability and/or AOLP decrease during or shortly after a glint. Since the polarization signature outside of the glint is heavily influenced by reflections off the spacecraft bus, while the glinting polarization signature corresponds primarily to reflections off the satellite's solar panels [10, 12], variations between satellite bus type and solar panel combinations may subtly impact a satellite's contrasting polarization signature between glint and non-glint phases. These differences may be leveraged to help discriminate between unresolved GEO objects.

5. CONCLUSIONS

The work presented in this paper is a step towards better characterizing satellites using near-simultaneous polarization measurements. This paper focused on determining whether unresolved linear polarization data can be used to characterize satellites. We observed six operational geosynchronous communication satellites (AMC-15, Wildblue-1, SES-3, and DirecTV-10/14/15) during equinoctial periods from 2019 to 2021 and presented the total irradiance of their photometric signature (S_0) produced by their linear Stokes parameters (S_1 and S_2), degree-of-linear-polarization (DOLP), and angle-of-linear-polarization (AOLP). The DOLP and AOLP during a glint exhibited different features than the DOLP and AOLP outside of the glint period. We also studied the connection between satellite properties and their polarization signatures. We determined a correlation between the peak intensity of light reflected off a satellite during a glint and the corresponding glint DOLP, which is even stronger for a single class of satellites such as the DTV satellites. Further observations of satellites with different properties (e.g. relative size between solar panel and satellite bus) are warranted to see whether satellite attributes can be predicted or determined with unresolved polarization measurements. Additionally, more data is needed before and after satellite glints to better understand variations in AOLP throughout the night. We intend to extend this study to other times of the year in order to determine seasonal effects on a satellite's polarization signature.

We also developed a technique to determine whether our polarization measurements are corrupted by clouds by correlating S_1 (or S_2) of one satellite versus S_1 (or S_2) of another satellite in the same image. A future project should examine whether we can extend this corrupt versus uncorrupt technique to images containing a single satellite by comparing the satellite polarization signature to multiple background signatures within the same image. Additionally, we need to extend this technique to varying time periods so that we can identify time periods for a night that has sporadic cloud cover without eliminating the entire night's worth of data.

6. ACKNOWLEDGEMENTS

We want to acknowledge the support of the Air Force Office of Scientific Research. Additionally, this paper is the result of multiple physics senior capstone projects and independent studies at the United States Air Force Academy since 2019. We especially want to acknowledge the following former cadets who collected some of the earlier satellite polarization observations: Cadet Marco Pirozzoli, Cadet Lucy Zimmerman, and Cadet Sequoia Chun. DISTRIBUTION STATEMENT A: Approved for public release: distribution unlimited. PA#: USAFA-DF-2021-254. DISCLAIMER: The views expressed in this article are those of the authors and do not necessarily reflect the

official policy or position of the United States Air Force Academy, the United States Air Force, the United States Space Force, the Department of Defense, or the U.S. Government.

7. REFERENCES

[1] Kirby, L. (2020, September 1). 2.4k Airmen to transfer into Space Force beginning Sept. 1. Retrieved September 7, 2020

[2] Scott, K. D. (2018, April 10). Joint Publication 3-14. Space Operations. Chairman of the Joint Chiefs of Staff. Retrieved September 6, 2020

[3] Raymond, J. W. (2020, August 10). Space Capstone Publication. Spacepower. Headquarters United States Space Force.

[4] Krebs, G. (2017, 11 12). Gunter's Space Page. Retrieved from Space.SkyRocket: https://space.skyrocket.de/doc_sdat/wildblue-1.htm

[5] Tousey, R., "Optical Problems of the Satellite," Journal of the Optical Society of America, 47, 261-267 (1957)

[6] Kissell, K.E. and Tyson, E.T., "Rapid-Response Photometry of Satellites," Astronomical Journal, 69, 547 (1964).

[7] Lambert, J.V., "Measurement of the Visible Reflectance Spectra of Orbiting Satellites," M.S. Thesis, Air Force Institute of Technology (1971).

[8] Payne, T. E., Gregory, S. A., Houtkooper, N. M., and Burdullis, T. W., "Classification of Geosynchronous Satellites Using Photometric Techniques," Proceedings of the 2002 AMOS Technical Conference, The Maui Economic Development Board, Inc., Kihei, Maui, HI (2002).

[9] Payne, T. E., Gregory, S. A., and Luu, K., "SSA Analysis of GEOS Photometric Signature Classifications and Solar Panel Offsets," Proceedings of the 2006 AMOS Technical Conference, The Maui Economic Development Board, Inc., 667-673 (2006).

[10] Vrba, F.J., DiVittorio, M.E., Hindsley, R.B., Schmitt, H.R., Armstrong, J.T., Shankland, P.D., Hutter, D.J., and Benson, J.A., "A survey of geosynchronous satellite glints." The 2009 AMOS Technical Conference Proceedings, The Maui Economic Development Board, Inc., Kihei, Maui, HI (2009).

[11] Schildknecht, T., Vananti, A., Krag, H., and Erd, C., "Reflectance spectra of space debris in GEO," The 2009 AMOS Technical Conference Proceedings, The Maui Economic Development Board, Inc., Kihei, Maui, HI, 220-227 (2009).

[12] Dunsmore, A.N., J.A. Key, R.M. Tucker, E.M. Weld, F.K. Chun, and R.D. Tippets, "Spectral Measurements of Geosynchronous Satellites During Glint Season," J. Spacecraft and Rockets, (2016). doi: http://arc.aiaa.org/doi/abs/10.2514/1.A33583.

[13] D. Bédard, G. Wade, D. Monin, and R. Scott, "Spectrometric characterization of geostationary satellites," Proceedings of the 2012 AMOS Technical Conference, The Maui Economic Development Board, Inc., Kihei, Maui, HI (2012).

[14] Stead, R.P., "An Investigation of Polarization Phenomena Produced by Space Objects," M.S. Thesis, GSP/PH/67-7, Air Force Institute of Technology, Wright-Patterson Air Force Base, Ohio, 1967.

[15] Speicher, J.A., "Identification of Geostationary Satellites Using Polarization Data from Unresolved Images." PhD Dissertation, University of Denver, 2015.

[16] Brewster's Angle. (n.d.). Retrieved from RP Photonics Encyclopedia: https://www.rp-photonics.com/brewsters_angle.html

[17] Lazos, D. (2018). HSC Physics New Syllabus 2018: Top 5 Changes. Retrieved from TutorPro: https://tutorpro.com.au/hsc-physics-new-syllabus/

[18] Pirozzoli, M.F., L.A. Zimmerman, M. Korta, A.D. Scheppe, M.K. Plummer, F.K. Chun, D.M. Strong, "Calibration and sensitivity analysis of a basic polarimeter for manmade satellite observations," The 2020 AMOS Technical Conference Proceedings, The Maui Economic Development Board, Inc., Kihei, Maui, HI, 2020.

[19] Pirozzoli, M.F., L.A. Zimmerman, M. Korta, A.D. Scheppe, F.K. Chun, D.M. Strong, M.K. Plummer, and C.N. Harris,, "Characterization of Unresolved Satellite Imagery Using Polarization Data," Winter Meeting of the American Astronomical Society, Honolulu, HI, January 2020.

[20] Zimmerman, L.A., S.S. Chun, M.F. Pirozzoli, D.M. Strong, M.K. Plummer, and F.K. Chun, "Near-Simultaneous Polarization and Spectral Optical Measurements of Geosynchronous Satellites," The 2020 AMOS Technical Conference Proceedings, The Maui Economic Development Board, Inc., Kihei, Maui, HI, 2020